Inorg. Chem. **2008**, *47*, 11543−11550

Geometric Structure Determination of N694C Lipoxygenase: A Comparative Near-Edge X-Ray Absorption Spectroscopy and Extended X-Ray Absorption Fine Structure Study

Ritimukta Sarangi,[||] Rosalie K. Hocking,[†] Michael L. Neidig,[†] Maurizio Benfatto,*[,‡] Theodore R. Holman,[§] Edward I. Solomon,[†,||] Keith O. Hodgson,[†,||] and Britt Hedman*[,||]

Department of Chemistry, Stanford University, Stanford, California 94305, Laboratori Nazionali di Frascati dell' INFN, C.P. 13, 00044 Frascati, Italy, Department of Chemistry and Biochemistry, University of California, Santa Cruz, California 95064, and Stanford Synchrotron Radiation Laboratory, SLAC, Stanford University, Stanford, California 94309

Received April 1, 2008; Accepted June 11, 2008; Revised Manuscript Received June 10, 2008

The mononuclear nonheme iron active site of N694C soybean lipoxygenase (sLO1) has been investigated in the resting ferrous form using a combination of Fe−K-pre-edge, near-edge (using the minuit X-ray absorption near-edge full multiple-scattering approach), and extended X-ray absorption fine structure (EXAFS) methods. The results indicate that the active site is six-coordinate (6C) with a large perturbation in the first-shell bond distances in comparison to the more ordered octahedral site in wild-type sLO1. Upon mutation of the asparigine to cystiene, the short Fe−O interaction with asparigine is replaced by a weak Fe−(H_2O), which leads to a distorted 6C site with an effective 5C ligand field. In addition, it is shown that near-edge multiple scattering analysis can give important three-dimensional structural information, which usually cannot be accessed using EXAFS analysis. It is further shown that, relative to EXAFS, near-edge analysis is more sensitive to partial coordination numbers and can be potentially used as a tool for structure determination in a mixture of chemical species.

1. Introduction

Extended X-ray absorption fine structure (EXAFS) is a powerful technique for local structure determination on systems in both solution and solid (amorphous and crystalline) states.[1−3] Traditionally, EXAFS has been applied to a broad range of scientific fields, especially for systems that cannot be obtained in the crystalline form for X-ray diffraction measurements. The EXAFS region typically extends from ∼50 to 1500 eV above the edge inflection of the X-ray absorption spectrum; however, the magnitude of the EXAFS signal is reduced rapidly with energy. This imposes potential limitations; for example, (*i*) at low absorber concentrations, sufficient signal-to-noise ratios at higher energies may not be obtained, constraining the data range; (*ii*) photoreduction and beam damage may impair multiple scan averaging for low-concentration samples or (*iii*) inherently weak EXAFS signals, which inhibit data collection to high energies. These limitations are in particular applicable to nonheme iron proteins, which usually have irregular first-shell (N/O) ligation and cannot be obtained at higher concentrations.[3] The near-edge region of an X-ray absorption spectroscopy (XAS) spectrum (∼ −10 to +200 eV) successfully overcomes the concentration and weak signal limitations in such systems. Also, since good-quality near-edge data can be collected significantly faster, beam damage and photoreduction can be minimized. The near-edge fitting methodology implemented into the MXAN code (minuit X-ray absorption near-edge), which has been developed by Benfatto et al., has been successfully applied to several small inorganic molecules.[4−7] In a recent study, the full multiple scattering

* Authors to whom correspondence should be addressed. E-mail: hedman@ssrl.slac.stanford.edu (B.H.); Maurizio.Benfatto@lnf.infn.it (M.B).
[||] Stanford Synchrotron Radiation Laboratory.
[†] Department of Chemistry, Stanford University.
[‡] Laboratori Nazionali di Frascati dell' INFN.
[§] University of California.

(1) Stern, E. A. In *EXAFS, SEXAFS and XANES*; Koningsberger, D. C., Prins, R., Eds.; John Wiley & Sons: New York: 1988; Vol. *1*.
(2) Teo, B. K. *EXAFS: Basic Principles and Data Analysis*; Springer-Verlag: New York, 1986.
(3) Zhang, H. H.; Hedman, B.; Hodgson, K. O. In *Inorganic Electronic Structure and Spectroscopy*; Solomon, E. I., Lever, A. B. P., Eds.; John Wiley & Sons: New York: 1999; Vol. *1*, pp 514−554.
(4) Benfatto, M.; Della Longa, S. *J. Synchrotron Radiat.* **2001**, *8*, 1087–1094.

10.1021/ic800580f CCC: $40.75
Published on Web 07/26/2008

theory implemented in MXAN was applied to [Cu(TMPA)-(OH_2)](ClO_4), which is a model complex that mimics the active site of cytochrome *c* oxidase.[8] It was shown that MXAN was successful in simulating the near-edge spectrum and in describing the complex multiple-scattering from the TMPA ligand system. In addition, it was shown that the multiple scattering approach is sensitive to small structural and angular variations.

Lipoxygenases (LOs),[9–13] which are nonheme iron-containing enzymes with mixed N/O donor ligands, are systems challenged by the above-mentioned EXAFS limitations. Although two different crystal structures of soybean lipoxygenase (sLO) have described the resting ferrous active site as six-coordinate (6C; three histidine ligands (His), the C-terminal isoleucine (Ile) ligated to the Fe with the free carboxylate oxygen, H_2O, and a weakly coupled asparigine (Asn) ligand)[14,15] and strongly distorted four-coordinate (4C; considering only the four strongly coordinating first-shell ligands, i.e., three His and the free carboxylate oxygen of the C-terminal Ile),[16] a combination of circular dichroism (CD) and magnetic circular dichroism (MCD) studies,[17] which is a powerful technique to identify the coordination number on the basis of a ligand field analysis, indicated that the ferrous site is a mixture of five-coordinate (5C) and 6C, in a 40/60 ratio which becomes 6C upon glycerol addition. This has been confirmed by EXAFS measurements on wild-type (WT) sLO in the presence of 30% glycerol.[17]

In this study, the MXAN near-edge multiple-scattering method has been used, at the Fe−K edge, in combination with pre-edge and EXAFS analysis to study the ferrous form of the N694C mutant of lipoxygenase. In this mutant, the weakly coordinating first-coordination sphere amino acid Asn694 has been replaced by a potentially strongly coordinating cysteine ligand. CD and MCD studies indicate that the ferrous site is 5C and remains 5C upon glycerol binding.[18] However, in the absence of a crystal structure, there are several structural possibilities for a 5C site. These structural possibilities (elaborated in the Results and Analysis section) have been evaluated using this combined XAS analysis approach. The results indicate that the active site is distorted 5 + 1C with a weakly coordinated axial H_2O at an Fe−O distance of 2.5 Å, and that this weak coordination of the water molecule to the ferrous center retains an approximately 5C ligand field (in the presence of glycerol). It is shown that the near-edge multiple scattering approach can differentiate between structural models proposed by EXAFS and can be used as a powerful structural tool if adequate EXAFS data are not available.

2. Experimental Section

2.1. Sample Preparation. Site-directed mutagenesis, overexpression, and purification of N694C sLO followed a protocol outlined previously.[19] N694C was purified with a yield of 2−4 mg/L, with a metal content of 55 ± 10%. N694C was concentrated, and 30% (v/v) glycerol was added to form an optical quality glass with a final Fe^{II} concentration of ~1 mM. The enzyme sample was then transferred under an inert atmosphere wet-box to an XAS sample cell and frozen immediately in liquid nitrogen.

2.2. X-Ray Absorption Spectroscopy. The X-ray absorption spectra of the N694C mutant of LO were measured at the Stanford Synchrotron Radiation Laboratory on the focused 16-pole 2.0 T wiggler beam line 9-3 and the unfocused eight-pole 1.8 T wiggler beam line 7-3 under standard ring conditions of 3 GeV and 60−100 mA. A Si(220) double-crystal monochromator was used for energy selection. A Rh-coated harmonic rejection mirror and a cylindrical Rh-coated bent focusing mirror were used for beam line 9-3, whereas the monochromator was detuned 50% at 7998 eV on beam line 7-3 to reject components of higher harmonics. The protein solutions were loaded into 1 mm lucite XAS cells with X-ray transparent ~37 μm Kapton windows. The samples were immediately frozen thereafter and stored under liquid N_2 conditions. During data collection, the sample was maintained at a constant temperature of 10 K using an Oxford Instruments CF 1208 liquid helium cryostat. The fluorescence mode was used to measure data to $k = 15$ Å^{-1} using a 30-element Ge solid-state detector windowed on the Fe−Kα signal. Internal energy calibration was accomplished by simultaneous measurement of the absorption of an Fe-foil placed between two ionization chambers situated after the sample. The first inflection point of the foil spectrum was assigned to 7111.2 eV.

Data represented here are a 21-scan average spectrum, which was processed by fitting a second-order polynomial to the pre-edge region and subtracting this from the entire spectrum as background. A three-region spline on the of orders 2, 3, and 3 was used to model the smoothly decaying post-edge region. The data were normalized by subtracting the cubic spline and by assigning the edge jump to 1.0 at 7120 eV using the *SPLINE* program in the XFIT suite of programs.[20]

2.3. Pre-Edge Data Analysis. Least-squares fits were performed using the *EDG_FIT* program[21] to quantify the intensity and energy of the pre-edge feature. The pre-edge features were modeled using 50:50 Lorentzian/Gaussian pseudo-Voigt functions. The rising-edge background was modeled using a pseudo-Voigt function, which

(5) Benfatto, M.; Della Longa, S.; D'Angelo, P. *Phys. Scr.* **2005**, *T115*, 28–30.
(6) Benfatto, M.; Della Longa, S.; Natoli, C. R. *J. Synchrotron Radiat.* **2003**, *10*, 51–57.
(7) Hayakawa, K.; Hatada, K.; D'Angelo, P.; Della Longa, S.; Natoli, C. R.; Benfatto, M. *J. Am. Chem. Soc.* **2004**, *126*, 15618–15623.
(8) Sarangi, R.; Benfatto, M.; Hayakawa, K.; Bubacco, L.; Solomon, E. I.; Hodgson, K. O.; Hedman, B. *Inorg. Chem.* **2005**, *44*, 9652–9659.
(9) Ford-Hutchinson, A. W.; Gresser, M.; Young, R. N. *Annu. Rev. Biochem.* **1994**, *63*, 383–417.
(10) Glickman, M. H.; Klinman, J. P. *Biochemistry* **1996**, *35*, 12882–12892.
(11) Solomon, E. I.; Brunold, T. C.; Davis, M. I.; Kemsley, J. N.; Lee, S. K.; Lehnert, N.; Neese, F.; Skulan, A. J.; Yang, Y. S.; Zhou, J. *Chem. Rev.* **2000**, *100*, 235–349.
(12) Brash, A. R. *J. Biol. Chem.* **1999**, *274*, 23679–23682.
(13) Solomon, E. I.; Zhou, J.; Neese, F.; Pavel, E. G. *Chem. Biol.* **1997**, *4*, 795–808.
(14) Minor, W.; Steczko, J.; Stec, B.; Otwinowski, Z.; Bolin, J. T.; Walter, R.; Axelrod, B. *Biochemistry* **1996**, *35*, 10687–10701.
(15) Tomchick, D. R.; Phan, P.; Cymborowski, M.; Minor, W.; Holman, T. R. *Biochemistry* **2001**, *40*, 7509–7517.
(16) Boyington, J. C.; Gaffney, B. J.; Amzel, L. M. *Science* **1993**, *260*, 1482–1486.
(17) Pavlosky, M. A.; Zhang, Y.; Westre, T. E.; Gan, Q.-F.; Pavel, E. G.; Campochiaro, C.; Hedman, B.; Hodgson, K. O.; Solomon, E. I. *J. Am. Chem. Soc.* **1995**, *117*, 4316–4327.
(18) Neidig, M. L.; Wecksler, A. T.; Schenk, G.; Holman, T. R.; Solomon, E. I. *J. Am. Chem. Soc.* **2007**, *129*, 7531–7537.
(19) Holman, T. R.; Zhou, J.; Solomon, E. I. *J. Am. Chem. Soc.* **1998**, *120*, 12564–12572.
(20) Ellis, P. J.; Freeman, H. C. *J. Synchrotron Radiat.* **1995**, *2*, 190–195.
(21) George, G. N. *EXAFSPAK & EDG_FIT*; Stanford Synchrotron Radiation Laboratory, Stanford Linear Accelerator Center, Stanford University: Stanford, CA, 2000.

mimicked the white line associated with the edge transition. Additional pseudo-Voigt peaks were also used to mimic shoulders on the rising edge. The data were fit over several different energy regions. The least-squares error and a comparison of the second derivatives of the data and fit were used to determine the goodness of fit. The standard deviations in energy and intensity over all successful fits were used to quantify errors in these parameters.

2.4. Near-Edge Data Analysis. The near-edge simulations were performed using MXAN,[4,7] which performs a full multiple-scattering analysis of the data to obtain structural information.[7,22] The following programs are integrated in MXAN: VGEN, a generator of muffin-tin potential, the CONTINUUM code for full multiple-scattering cross-section calculation, and the MINUIT routines of the CERN library for parameter optimization. The starting structures used in the simulations were generated by modifying the crystal structure of wild-type sLO.[15] Several starting structures were considered, which included both 5C and 6C Fe centers. The data were fit over the −5 to +190 eV energy range (0 eV is defined at 7130 eV). In the refinement, all atoms belonging to the histidine rings were moved rigidly linked to the N atom coordinated to the Fe. In the first step of the optimization process, only the bond distances were allowed to float. In subsequent steps, the dihedral angles were also allowed to float. After each step of structural parameter refinement, a nonstructural parameter refinement was performed. Many applications of MXAN to small molecule XAS data indicate that the correlation between structural and nonstructural parameters is small. Nevertheless, the refinements were closely monitored for any large fluctuations in the structural and nonstructural parameters during the refinement process. No large deviations in either the structural or the nonstructural parameters were observed. The least-squares error and a visual comparison of data and fit were used to determine the goodness of fit.

2.5. EXAFS Data Analysis. Theoretical EXAFS signals $\chi(k)$ were calculated using *FEFF* (version 7.0)[23,24] and the crystal structure of wild-type LO as the initial model, and they were fit to the data using EXAFSPAK (G. N. George, SSRL).[21] Theoretical paths corresponding to Fe−S and Fe−O distances of 2.1−3.0 Å (in 0.1 Å steps) were also calculated to simulate contributions of the S(Cys) to the EXAFS signal. For both paths, the best fit distance was added to the active site in the crystal structure of wild-type LO, a new set of theoretical $\chi(k)$'s was calculated using *FEFF*, and the data were refit using the new parameters. The structural parameters varied during the fitting process were the bond distance (R) and the bond variance (σ^2), which is related to the Debye−Waller factor resulting from thermal motion, and static disorder. The nonstructural parameter E_0 (the energy at which $k = 0$) was also allowed to vary but was restricted to a common value for every component in a given fit. Coordination numbers were systematically varied in the course of the fit but were fixed within a given fit.

3. Results and Analysis

3.1. Fe−K Pre-Edge. The Fe−K pre-edge results from a quadrupole-allowed dipole-forbidden 1s → 3d transition. These transitions are usually very weak (~100 times weaker than the edge) but can gain intensity when the coordination deviates from centrosymmetry and gains dipole-allowed

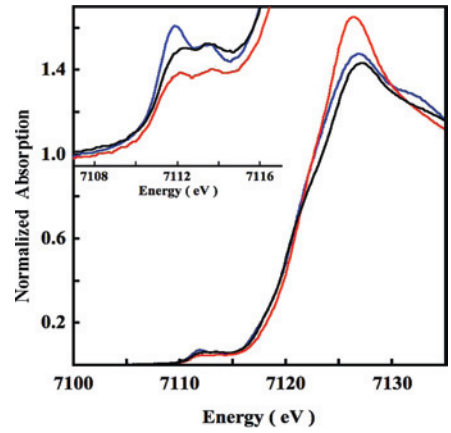

Figure 1. The normalized Fe−K near-edge region of N694C LO (black), PAH^R (blue), and PAH^T (red). Inset shows the expanded pre-edge region.

character due to Fe 4p mixing into the Fe 3d orbitals, as 1s → 4p transitions are electric-dipole-allowed.[25] It has been shown by extensive studies on small molecule model complexes that the energy position and intensity pattern of the pre-edge transitions are signatures of the oxidation state and ligand coordination, respectively.[25−27] Ferrous 6C (O_h) complexes typically have a total integrated area of ~4 units over the pre-edge transition range. In 4C and 5C complexes, the center of inversion is absent, leading to more intense pre-edge transitions, typically by a factor of 3−4. The 4C and 5C complexes can be differentiated on the basis of the intensity distribution of the pre-edge transitions.

The Fe−K pre-edge spectrum of ferrous N694C LO is compared to that of ferrous PAH^T (wild-type phenylalanine hydroxylase (PAH)) and PAH^R (substrate- and cofactor-bound PAH) in Figure 1 (inset).[28] It has been shown using X-ray absorption, CD, and MCD studies that the Fe centers in PAH^T and PAH^R are 6C and 5C, respectively.[29] The total integrated area under the pre-edge transitions of N694C LO, PAH^T, and PAH^R are 11.8(0.4), 8.1(0.4), and 13.9(0.8), respectively.[30] The individual peak energy and intensity of N694C LO, PAH^T, and PAH^R are listed in Table 1. The total integrated intensity of N694C LO is similar to that of PAH^R, indicating that the active site Fe is 5C. These results are consistent with MCD data for N694C LO, which also indicate that the active site in N694C LO is consistent with a 5C ligand field.[18] However, the intensity ratio of the two pre-edge features is 1.44, which is closer to a 6C complex than a 5C complex (the intensity ratios of the pre-edge features in PAH^R and PAH^T are 1.61 and 1.39, respectively, see Figure S1, Supporting Information). In strictly 5C C_{4v}

(22) Tyson, T. A.; Hodgson, K. O.; Natoli, C. R.; Benfatto, M. *Phys. Rev. B: Condens. Matter Mater. Phys.* **1992**, *46*, 5997–6019.
(23) Mustre de Leon, J.; Rehr, J. J.; Zabinsky, S. I.; Albers, R. C. *Phys. Rev. B: Condens. Matter Mater. Phys.* **1991**, *44*, 4146–4156.
(24) Rehr, J. J.; Mustre de Leon, J.; Zabinsky, S. I.; Albers, R. C. *J. Am. Chem. Soc.* **1991**, *113*, 5135–5140.
(25) Westre, T. E.; Kennepohl, P.; DeWitt, J. G.; Hedman, B.; Hodgson, K. O.; Solomon, E. I. *J. Am. Chem. Soc.* **1997**, *119*, 6297–6314.
(26) Randall, C. R.; Shu, L. J.; Chiou, Y. M.; Hagen, K. S.; Ito, M.; Kitajima, N.; Lachicotte, R. J.; Zang, Y.; Que, L., Jr. *Inorg. Chem.* **1995**, *34*, 1036–1039.
(27) Roe, A. L.; Schneider, D. J.; Mayer, R. J.; Pyrz, J. W.; Widom, J.; Que, L., Jr. *J. Am. Chem. Soc.* **1984**, *106*, 1676–1681.
(28) The pre-edge data for PAH^T and PAH^R have been reproduced from ref 29.
(29) Wasinger, E. C.; Mitíc, N.; Hedman, B.; Caradonna, J.; Solomon, E. I.; Hodgson, K. O. *Biochemistry* **2002**, *41*, 6211–6217.
(30) The Fe−K pre-edge data of the 6C site in PAH^T has been refit with two peaks to determine the intensity ratio.

Table 1. Fe−K Pre-Edge Analysis[a]

	N694C-LO	PAH^R	PAH^T[b]
peak 1 (eV)	7111.7	7111.7	7111.8
peak 2 (eV)	7113.5	7113.5	7113.7
total area[c]	11.8(0.4)	13.9(0.8)	8.1(0.4)
pre-edge ratio	1.44	1.61	1.39
edge maxima (eV)	7126.3	7126.4	7125.7

[a] Values in parentheses are the statistical standard deviations calculated from the individual acceptable fits used in the analysis. [b] The first two peaks in PAH^T are in the limit of resolution and hence treated as a single peak for relative ratio estimations. [c] The reported values are multiplied by 100 for convenience.

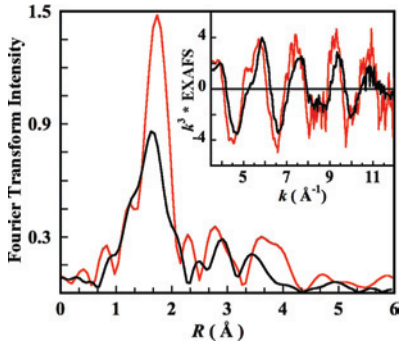

Figure 2. Fourier transforms (non-phase-shift-corrected) and EXAFS data (inset). N694C LO (black) and WT-LO (red).

complexes, the lower-energy pre-edge feature associated with an Fe 1s → d_{z^2} (A_1 symmetry) transition gains intensity due to Fe $4p_z$ (A_1 symmetry) mixing with the d_{z^2} orbital. However, in protein environments, the active site can deviate considerably from an ideal C_{4v} geometry due to differences in ligands or the presence of a weak sixth ligand.[31] This lowers the symmetry, and the higher-energy pre-edge feature can also gain intensity through Fe $4p_{x,y}$ mixing with the $d_{x^2-y^2}$ orbital. This indicates that the active site in N694C LO is more distorted than that in PAH^R.

Figure 1 shows a comparison of the rising edge regions of N694C LO, PAH^T, and PAH^R. The intensity of the peak at ~7126 eV is lower and similar for N694C LO and PAH^R compared to PAH^T. Since the intensity of this peak is characteristic of the number and type of first-shell ligands,[32] the edge data of N694C LO indicate a ligand field consistent with a 5C structure and with the pre-edge data and MCD studies.

3.2. EXAFS Region. The EXAFS data for N694C LO were Fourier-transformed over $k = 2-12.5$ Å^{-1}. The EXAFS and the Fourier transform data are compared with those of the WT sLO in Figure 2.[33] The EXAFS for WT sLO has a phase-shift to lower k relative to N694C sLO, similar to the relative phase shift in PAH^T (6C) and PAH^R (5C).[29] The first-shell Fourier transform intensity has decreased by almost a factor of 2 in N694C LO relative to WT sLO. Both the WT sLO and N694C sLO data were collected in the presence of ~30% glycerol as the glassing agent. In the case of WT

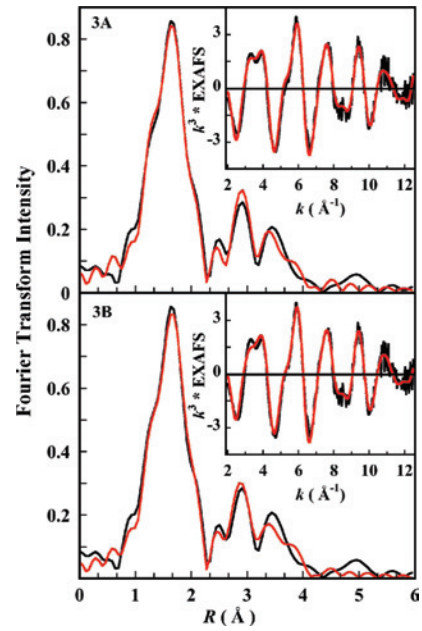

Figure 3. Fourier transforms (non-phase-shift-corrected) and EXAFS data (inset) for N694C LO. (A) Best fit using the Fe/S model. (B) Best fit using the Fe/O model (see text for more details). Data (black) and fit (red).

sLO, it has been shown using CD, MCD, and K-pre-edge studies that, in the presence of glycerol (or alcohols), the active site structure shifts from a 5C/6C (40%/60%) mixture to a purely 6C form. First-shell Fourier-filtered EXAFS fits were also consistent with these results, indicating six Fe−O/N contributions at ~2.16 Å.[17] The EXAFS fits have been refined here using a full multiple scattering approach. The best fit to the WT-LO EXAFS and the corresponding Fourier transforms are presented in Figure S2 (Supporting Information), with the fit parameters given in Table S1 (Supporting Information). The first shell is fit using six Fe−O/N contributions at 2.18 Å.

In N694C LO, asparigine 694 is replaced by a cysteine residue. Thus, the weakly coordinating amide oxygen is replaced by a thiolate S(Cys) group which can potentially coordinate strongly with the Fe atom. However, due to the smaller size of S(Cys) relative to O(Asn), its approach to the ferrous center is restricted by the backbone in N694C sLO, compared to the more flexible approach of the amide O of asparigine in the WT sLO. This might create a possible pocket for a H_2O molecule in N694C sLO, which can coordinate to the Fe atom as a sixth ligand.[34] Both of these possibilities were explored using appropriate models to generate theoretical EXAFS signals $\chi(k)$ using *FEFF*. The fits to the EXAFS data using both of these models and the corresponding Fourier transforms are shown in Figure 3A and B. The best-fit parameters are presented in Table 2. The Fe/S model was generated by including an Fe−S contribution at 2.7 Å in the input structure.[35] Using this model, the first shell was fit using one Fe−O/N path at 1.97 Å, four Fe−O/N

(31) Davis, M. I.; Wasinger, E. C.; Westre, T. E.; Zaleski, J. M.; Orville, A. M.; Lipscomb, J. D.; Hedman, B.; Hodgson, K. O.; Solomon, E. I. *Inorg. Chem.* **1999**, *38*, 3676–3683.
(32) DeWitt, J. G.; Rosenzweig, A. C.; Salifoglou, A.; Hedman, B.; Lippard, S. J.; Hodgson, K. O. *Inorg. Chem.* **1995**, *34*, 2505–2515.
(33) The EXAFS data for WT sLO1 presented here have been previously reported in ref 17.
(34) Segraves, E. N.; Chruszcz, M.; Neidig, M. L.; Ruddat, V.; Zhou, J.; Wecksler, A. T.; Minor, W.; Solomon, E. I.; Holman, T. R. *Biochemistry* **2006**, *45*, 10233–10242.
(35) Several Fe/S models with an Fe−S distance ranging from 2.5 to 3.0 Å were used to generate theoretical paths. The best fit was obtained using the model with an Fe−S distance of ~2.7 Å.

Table 2. EXAFS Least-Squares Fitting Results for N694C Lipoxygenase

fit #	coordination/path	R (Å)[a]	σ^2 (Å^2)[b]	E_0 (eV)	F[c]
model Fe/S	1 Fe−N/O	1.97(0.02)	259(48)	−6.99	0.135
	4 Fe−N/O	2.12(0.02)	442(202)		
	1 Fe−S	2.70(0.03)	1300(131)		
	6 Fe−C	3.12(0.02)	557(44)		
	14 Fe−N−C	3.27(0.02)	557[d](44)		
	8 Fe−N/C−N/C	4.29(0.04)	163(190)		
	8 Fe−N/C−N/C	4.44(0.03)	719(190)		
model Fe/O	1 Fe−N/O	1.96(0.03)	420(113)	−7.99	0.138
	4 Fe−N/O	2.12(0.02)	520(66)		
	1 Fe−O/N	2.49(0.02)	542(121)		
	6 Fe−C	3.11(0.02)	725(65)		
	14 Fe−N−C	3.29(0.04)	725(65)		
	8 Fe−N/C−N/C	4.28(0.04)	279(240)		
	8 Fe−N/C−N/C	4.41(0.02)	855(240)		

[a] The estimated standard deviations for the distances and σ^2 parameters calculated by EXAFSPAK are shown in parantheses. [b] The σ^2 values are multiplied by 10^5. [c] Error is given by $\sum[(\chi_{obsd} - \chi_{calcd})^2 k^6]/\sum[(\chi_{obsd})^2 k^6]$. [d] The σ^2 factor of the multiple scattering path is linked to that of the corresponding single scattering path. The S_o^2 value was fixed at 1 for all refinements.

paths at 2.12 Å,and one Fe−S at 2.70 Å.[36] The second and third shells were fit using single and multiple scattering contributions arising from the histidine ring N and C atoms. The σ^2 value for the Fe−S path (Table 2) was high, indicating that, if present, the long Fe−S contribution is disordered. Fits using a coordination number of less than 1 for the Fe−S path improved the σ^2 value but did not affect the goodness of the fit, consistent with a putative disordered Fe−S bond. For the fits to the Fe/O model, which was generated using a structure that included an Fe−O path at 2.5 Å, the best fit was consistent with one Fe−O path at 1.96 Å, four Fe−O/N paths at 2.12 Å, and one Fe−O path at 2.49 Å. The second and third shells were fit using single and multiple scattering contributions arising from the histidine ring N and C atoms. Good fits were obtained when the third shell was modeled with two sets of eight Fe−N/C−N/C multiple scattering components (adding the single scattering path did not improve the fit). However, the correlations between the bond distances and the σ^2 factors for these two multiple scattering paths were quite high, which might lead to the unusually low σ^2-factor value for the multiple scattering path at 4.28/4.29 Å. The correlation matrices obtained from the EXAFS fits to both the Fe/O and Fe/S models are included in the Supporting Information (bond distance = correlation between parameters 32 and 37; σ^2 values = correlation parameters 33 and 38).

The σ^2 value of the Fe−O path at 2.5 Å is moderately high, which also indicates that, if the O is present, the Fe−O bond is disordered. The goodness of fit was very similar for both the Fe/S and Fe/O models. Thus, the EXAFS study indicates that the first shell is composed of one plus four Fe−N/O paths and a weakly coordinated Fe−O or Fe−S path, which is disordered. This is consistent with the observed intensity distribution and the total area for the pre-edge transitions, since a five-coordinate site with a weak sixth interaction would have a symmetry lower than O_h and would gain allowed character from 4p mixing into the 3d manifold, which would increase the intensity, and the presence of a weak interaction would change the intensity distribution from that observed for a pure C_{4v} species.

(36) A strong Fe−S(Cys) bond could lead to weakening of the H_2O ligand bond, leading to a distorted 5C structure with four Fe−O/N, one Fe−S, and one long Fe−O interaction. However, EXAFS data could not be reasonably fit using a structural model reflecting this geometry.

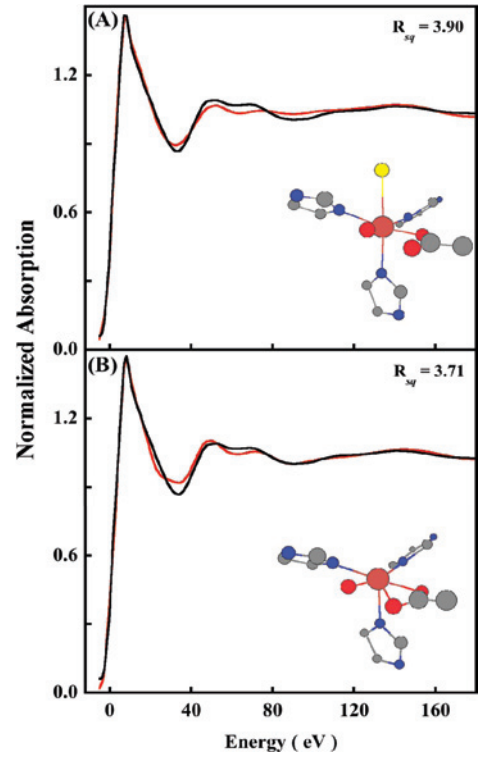

Figure 4. The normalized Fe−K near-edge spectrum of N694C LO (black) and the best fit (red) obtained from the optimization of both structural and nonstructural parameters. (A) Fe/S fit. (B) Fe/O bidentate carboxylate fit.

Thus, the EXAFS analysis indicates that the structure is distorted 6C with a weak sixth ligand, which can either be a distant Fe−O or Fe−S interaction. The Fe−S interaction would result from the S(Cys694), while the Fe−O interaction could result from two possibilities: (*i*) a water molecule or (*ii*) reorientation of the ligated carboxylate group of the isoleucine to bind in an asymmetric bidentate fashion. Since the angular information available from EXAFS analysis is limited, both structural models for the Fe/O case are possible.

3.3. Near-Edge Region. To investigate the presence and nature of the weak sixth ligand, near-edge simulations were performed using MXAN, which uses a multiple scattering approach to simulate the edge region.[4] The N694C LO data were fit to 200 eV above the edge. Fits were first performed using the 5C active site structure obtained from the WT crystal structure. An iterative fit process of structural and nonstructural parameters was performed, with the goodness of fit assessed as the square residual error (R_{sq}).[8] The R_{sq} for the 5C fit was 1.2. Figure S3 (Supporting Information) shows the best fit using the 5C structure, with the structural parameters given in Table S2 (Supporting Information). Fits were then performed by using both the Fe/S and Fe/O models (see the EXAFS section). For the Fe/S model, the simulations were very sensitive to the inclusion of an Fe−S component between 2.3 and 3.0 Å, and the resultant fits were considerably worse (Figure 4A), with an R_{sq} value of 3.9. Compared

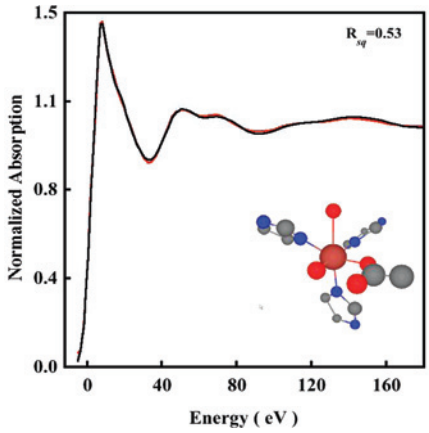

Figure 5. The normalized Fe−K near-edge spectrum of N694C LO (black) and the best fit (red) obtained from the optimization of both structural and nonstructural parameters using the Fe/O axial water model.

to the XAS spectra of a metal with O/N-only ligands, there is usually a dramatic change in the XAS spectra of metal−S-containing molecules, both in the rising edge and the near-edge region, which is usually associated with an increase in covalent interaction between the metal and sulfur. Since the near-edge fit results cannot accommodate an Fe−S interaction, it provides a clear indication that Cys694 is not ligated to Fe in the resting ferrous state. Using the Fe/O model, two input structures were generated. In the WT crystal structure, the carboxylate group (Ile) is asymmetrically coordinated with one Fe−O at 2.28 Å and the second Fe−O at 3.49 Å. The loss of the Asn ligand in N694C sLO might lead to a perturbation in the two Fe−O(Ile) bond distances, which can become shorter to compensate for the loss of the axial asparigine while still retaining their asymmetric coordination. Thus, the first input structure generated has two carboxylate Fe−O distances at 2.1 Å and 2.5 Å consistent with the two Fe−O bond distances obtained from the EXAFS data analysis. The second input structure consisted of a 6C structure with an axial Fe−O interaction at 2.5 Å representing an additional water molecule. Near-edge simulations using the asymmetric bidentate carboxylate structure resulted in an R_{sq} value of 3.7 (Figure 4B). This indicates that the carboxylate is coordinated in a monodentate fashion to the ferrous center with a sixth weak water ligand. Since the 6C fit with an asymmetric isoleucine carboxylate is worse than the 5C fit, near-edge simulations were performed with a sixth axial interaction at 2.5 Å (the equatorial plane is described by the two N(His), one O(Glu), and one O(H_2O)). It has been shown that such axial M−O bonds are sensitive to the dihedral angle made by the M−O bond with the equatorial plane.[8] Thus, the structure obtained from the 5C best fit was modified to obtain various 6C structures which included an Fe−O component at 2.5 Å and made different dihedral angles with the equatorial plane (see Figure S4, Supporting Information). These structures were then used to obtain structural and nonstructural fits to the near-edge data. Figure 5 shows the data and best-fit spectrum. The inset shows the optimized structure, and the structural parameters are presented in Table 2.[37] The best fit corresponds to an axial Fe−O distance of 2.50 Å, which is in good agreement with the EXAFS data. All of the other first-shell bond distances are in reasonable agreement with the EXAFS result. The R_{sq} value is 0.53, which is considerably better than that for the bidentate carboxylate and the Fe/S model, strongly indicating the presence of a weak long Fe−O coordination. It should be noted that, since the near-edge calculations are performed within the full multiple scattering approach, that is, since the inverse of the scattering path operator is computed exactly (avoiding any "a priori" selection of the relevant multiple scattering paths), the individual contribution of the histidine multiple scattering paths cannot be obtained. However, as seen from the insets in Figures 3 and 4 (and Cartesian coordinates given in the Supporting Information), the orientation of the histidine rings remains reasonably similar in fits to the Fe/O and Fe/S models, indicating that the increase in error value on going from the Fe/O to the Fe/S model results predominantly from the replacement of the Fe−O with the Fe−S contribution. It is interesting to note that fits to both the Fe/O and Fe/S models are reasonably good in the low R region in the EXAFS analysis but differ significantly in the near-edge analysis. This is accounted for by the following factors: (a) It has been previously observed that Fe−S contributions affect the edge significantly due to considerable changes in the electronic structure. This is exploited by the near-edge fitting routine implemented in MXAN, which calculates the inverse of the scattering path operator, exactly and treats the low-energy region better. (b) The σ^2 damping factor is not applicable to the near-edge fitting method using MXAN; thus, a "forced adjustment" of a longer Fe−S bond is not possible using a large σ value. (c) Finally, the EXAFS data are only available to $k = 12.5$ $Å^{-1}$ (typical for dilute nonheme iron proteins), which restricts our ability to distinguish between theoretically generated models with small differences.

Fits to EXAFS data usually give a 25% error in coordination number due to the strong correlation between the σ^2 value and the bond distance. In addition, partial coordination (the presence of a mixture of two components) can be explored using non-integer coordination numbers in the EXAFS fits. However, an exact two-component fit is currently unavailable in near-edge simulations using MXAN. To explore a 5C/6C mixture in N694C LO using near-edge simulations, a linear combination of the best fit 5 + 1C and the 5C model was performed within a window of 10% 6C/90% 5C and 90% 6C/10% 5C. These simulations were then compared to the data, and the error (ε) was obtained as $\varepsilon = \sum_{0-200eV} |S_{exp} - S_{sim}|$. Figure S5 (black line;Supporting Information) shows the change in error value with an increase in the 5C component. A corresponding EXAFS fit with non-integer Fe−O coordination was also performed, and the change in error value with an increase in the 5C component is shown in Figure S5 (red line; Supporting Information).

(37) The experimental and core-hole broadening values obtained from the non-structural parameter fit are 1.04 and 0.98 eV, respectively, yielding a total broadening of ~2 eV, which is consistent with the broadening observed at the Fe K-edge (~7100 eV).

These results clearly indicate that the molecule is 5 + 1C with no observable pure 5C component. Interestingly, the error for 10−50% 5C component (a higher amount of 5C component leads to unreasonable σ^2 values) remains very similar for the EXAFS fits, while that for MXAN shows a clear decrease in the goodness of fit. This indicates that edge-fitting is more sensitive to partial coordination number. Thus, these results emphasize the sensitivity of the multiple scattering method in fitting the near-edge region and obtaining geometric structure information, in particular angular information, which is usually inaccessible using EXAFS.

4. Discussion

4.1. Geometric Structure of N694C sLO1. In this study, a combination of pre-edge, near-edge, and EXAFS studies have been performed on N694C sLO to determine the active site geometric structure. These results indicate that the ferrous center is 5 + 1C with a weak Fe−O(H_2O) coordination at 2.5 Å. It is interesting to note that the MCD results indicate that the site is 5C with two ligand field bands at 6050 cm^{-1} and 11 450 cm^{-1}, although the MCD studies indicate a small increase in the ligand field on going from WT to N694C sLO. This discrepancy in the MCD and XAS results stems from the fact that a long Fe−O distance at 2.5 Å does not affect the bonding significantly enough to be seen as a coordination number change in MCD. However, the small shift in the MCD bands to higher energy indicates an increase in ligand field, reflecting a presence of a weak sixth ligand.

Both the WT and N694C sLO EXAFS data were measured in the presence of ∼30% glycerol. It has been shown in previous studies that glycerol converts the resting site 5C to 6C, which is similar to the structural change observed upon substrate binding.[17] This indicates that mutation of the weakly coordinated asparigine ligand to the smaller S(Cys) ligand removes the ability of the protein to convert into a 6C structure upon substrate binding. This is important in the reactivity of the protein since this 5C to 6C conversion, which is attributed to the coordination flexibility in the site, plays a key role in the catalytic rate. The weakly bound H_2O molecule keeps the site 5 + 1C in both resting and substrate-bound forms in N694C sLO1. The presence of this H_2O molecule likely modifies the H-bonding network between the second sphere residues by introducing a H bond between E697 and the H_2O molecule.[38] This H bond replaces the one lost between E697 and N694 due to mutation. Thus, although the substrate docking associated with the H-bond network might not be perturbed significantly, the substrate-bound active site structure (simulated by the presence of glycerol) changes dramatically between WT and N694C sLO, as observed from a comparison of the EXAFS data (see Figure 2). This leads to the observed ∼3000-fold decrease in the catalytic rate in N694C lipoxygenase relative to WT sLO.[18]

4.2. Comparison of Edge and EXAFS Analysis. The results presented in this study show that near-edge analysis can be used to complement EXAFS results and even give structural information inaccessible by EXAFS analysis. In N694C lipoxygenase, the two six-coordinate models involving a sixth oxygen atom, an axial water or a bidentate carboxylate of the Ile residue, can only be evaluated using a full multiple scattering approach, which is capable of determining three-dimensional structural information. At this point, it is important to evaluate the maximum number of independent parameters (I_P) and the reliability of the fit for the EXAFS and near-edge MXAN analysis. In the EXAFS region, I_P can be directly calculated using the relation $I_p = (2\Delta k \Delta R)/\pi + 2$.[39] For the N694C lipoxygenase EXAFS data, I_P is ∼20. The I_p number used in the EXAFS analysis presented here is 15, which is well within the upper limit of I_p that can be used to obtain an acceptable EXAFS fit.

In the edge region, however, since the mean free path of the photoelectron is very large, the multiple scattering contributions can extend up to ∼10 Å. This can exponentially increase the number of possible single- and multiple-scattering contributions to the edge region. Inclusion of all these paths can lead to structure-optimization problems since the possibility of reaching a local minimum for a system with a large number of independent parameters also increases rapidly. In the near-edge analysis presented here, single and multiple scattering contributions up to 4.5 Å have been considered, using 18 structural and 4 nonstructural parameters, respectively. It has been shown that the structural and nonstructural parameters have very low correlation; thus, the number of independent structural parameters in this analysis is ∼18. To justify the use of atoms up to 4.5 Å from the central ferrous atom, a shell-by-shell analysis is presented in Figure 6, which shows a multiple scattering contribution up to 2.6 Å (Figure 6A), 3.5 Å (Figure 6B), and 4.5 Å (Figure 6C, final fit). For each shell, the structural parameters were allowed to float. The 2.6 Å fit is very poor, with an R_{sq} of 6.5. While the 3.5 Å model reasonably fits the experimental spectral features (R_{sq} =1.7), the final 4.5 Å fit range (R_{sq} = 0.53) is essential to obtaining the double-peak feature between 50 and 80 eV. Thus, the results indicate that multiple-scattering contributions up to 4.5 Å are essential to successfully model the rising-edge and near-edge regions. This is in agreement with the EXAFS data, which require multiple-scattering contribution from C_β and N_β in the 4−4.5 Å range for a good fit. However, it is not sufficient to show that multiple-scattering contributions from atoms at a given distance are important to fit the edge data. Structural parameters in a fit can be highly correlated, leading to fits that do not represent the global minimum. The correlation matrix between the free parameters can be obtained using the MINUIT code implemented in the MXAN package, and that for the best fit shown in Figures 5 and 6C is presented in the Supporting Information. The matrix indicates low correlation between most parameters and supports the fact that the structural fit obtained using MXAN is physically justifiable. It is important to note that examination of the correlation matrix is important in EXAFS fitting procedures also and can give an estimate of the softness of the best-fit

(38) Schenk, G.; Neidig, M. L.; Zhou, J.; Holman, T. R.; Solomon, E. I. *Biochemistry* **2003**, *42*, 7294–7302.

(39) Stern, E. A. *Phys. Rev. B: Condens. Matter Mater. Phys.* **1993**, *48*, 9825–9827.

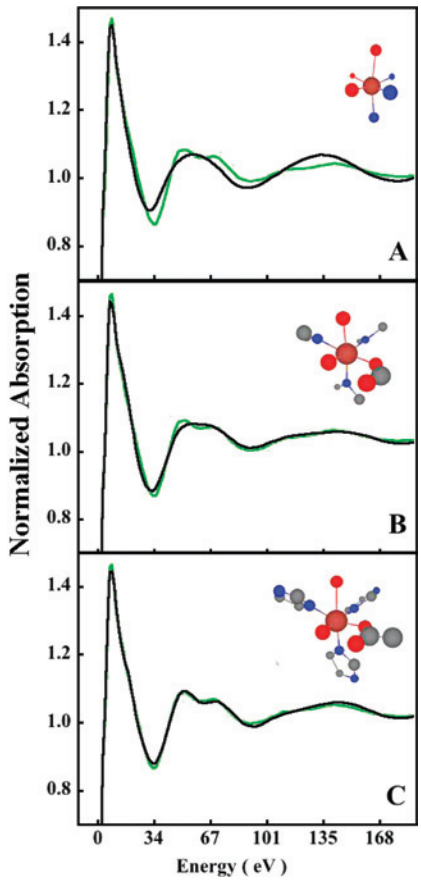

Figure 6. The normalized Fe−K near-edge spectrum of N694C LO (green) and the best fit (black) obtained from the optimization of both structural and nonstructural parameters using the best-fit model (six-coordinate Fe^{II} with axial water) up to 2.6 Å (A), 3.5 Å (B), and 4.5 Å (C).

structural parameters. Often, a particular bond distance in the EXAFS fit is closely correlated with its corresponding σ^2 value. Since the a priori estimation of σ^2 values for individual systems is not yet possible, an acceptable range of values is available for any particular absorber−scatterer pair on the basis of an EXAFS analysis on small models. However, this range of acceptable σ^2 values is quite large and, in some cases, can lead to large errors in bond-distance estimation, especially in the case of second- and third-shell single and multiple scattering. In most cases, a combination of chemical knowledge and close inspection of the statistical parameters at every step of the fitting process is important for accurate structure determination.

Table 3. Fe−K Edge Analysis[a]

path	Fe−O	Fe−O[c]	Fe−N_{eq}	Fe−N_{eq}	Fe−N_{ax}	Fe−O_{ax}
R (Å)	2.04	2.04	2.09	2.19	2.34	2.50

[a] The estimated standard deviation for the distances is ±0.01 Å and for bond angles (not shown) is 4°. [b] The structural and nonstructural parameters are obtained by alternate fitting of each set of parameters separately. This is possible due to the low correlation between these parameters. N_{ax} = axial N(His), N_{eq} = equatorial N(His). [c] Fe−OCO^-(Ile).

In summary, this study describes the application of a multiple-scattering edge-fitting methodology to a nonheme ferrous active site of the N694C mutant of lipoxygenase. It is shown that an edge-fitting analysis can give important three-dimensional structural information, which usually cannot be accessed using EXAFS analysis. In particular, for systems which are subject to limitations that can severely affect the resolution and accuracy of EXAFS analysis. In addition, since the σ^2 damping terms in the X-ray absorption near edge structure energy region are almost temperature-independent, atomic vibrations have negligible effects and do not interfere with structure determination. This allows a precise determination of partial coordination numbers and can be helpful in determining different compositions in mixtures.

Acknowledgment. This work was supported by NIH grants RR-01209 (K.O.H.), DK-31450 (E.I.S.), and GM56062-06 (T.R.H.). SSRL operations are funded by the Department of Energy, Office of Basic Energy Sciences. The SSRL Structural Molecular Biology program is supported by the National Institutes of Health, National Center for Research Resources, Biomedical Technology Program and by the Department of Energy, Office of Biological and Environmental Research. This publication was made possible by Grant 5 P41 RR001209 from the National Center for Research Resources (NCRR), a component of the National Institutes of Health (NIH). Its contents are solely the responsibility of the authors and do not necessarily represent the official view of NCRR or NIH.

Supporting Information Available: EXAFS fit results of WT sLO1. Near-edge fits to the 5C model of N694C sLO1. Structural model used to generate the 5C structure for N694C with a long axial water interaction. Comparison of change in square-residual errors with a change in 5C/5C+long axial ligation from near-edge and EXAFS analysis. This material is available free of charge via the Internet at http://pubs.acs.org.

IC800580F